

Quantum dot transistors based on CVD-grown graphene nano islands

Takumi Seo,^{1,2,*} Motoya Shinozaki,^{3,4,*} Akiko Tada,^{3,*} Yuta Kera,^{1,2} Shunsuke Yashima,^{1,2} Kosuke Noro,^{1,2,4} Takeshi Kumasaka,³ Azusa Utsumi,³ Takashi Matsumoto,⁵ Yoshiyuki Kobayashi,⁵ and Tomohiro Otsuka^{3,1,2,4,6,7,†}

¹Research Institute of Electrical Communication, Tohoku University, 2-1-1 Katahira, Aoba-ku, Sendai 980-8577, Japan

²Department of Electronic Engineering, Graduate School of Engineering, Tohoku University, Aoba 6-6-05, Aramaki, Aoba-Ku, Sendai 980-8579, Japan

³WPI Advanced Institute for Materials Research, Tohoku University, 2-1-1 Katahira, Aoba-ku, Sendai 980-8577, Japan

⁴Research Center for Materials Nanoarchitectonics (MANA),

National Institute for Material Science (NIMS), 1-2-1 Sengen, Tsukuba 305-0047, Japan

⁵S-Technology Development Center, Tokyo Electron Technology Solutions Limited, 650 Mitsuzawa, Hosaka-cho, Nirasaki, Yamanashi 407-0192, Japan

⁶Center for Science and Innovation in Spintronics, Tohoku University, 2-1-1 Katahira, Aoba-ku, Sendai 980-8577, Japan

⁷Center for Emergent Matter Science, RIKEN, 2-1 Hirosawa, Wako, Saitama 351-0198, Japan

Graphene nanoislands (GNIs) are one of the promising building blocks for quantum devices owing to their unique potential. However, direct electrical measurements of GNIs have been challenging due to the requirement of metal catalysts in typical synthesis methods. In this study, we demonstrate electrical transport measurements of GNIs by using microwave plasma chemical vapor deposition, which is a catalyst-free method to deposit graphene directly on SiO₂ substrates. This approach enables the fabrication of metal electrodes on GNIs, allowing us to measure their quantum transport properties. At low temperatures, one of our devices shows clear Coulomb diamonds with twofold degeneracy, indicating the formation of quantum dots and the vanishing of valley degeneracy. The charge state of the GNI is also modulated by a local side gate, and the tunneling coupling between leads and quantum dots is modulated by changing contact area and metal materials. These results provide device design guidelines toward GNI-based quantum devices for next-generation computing.

Graphene, a two-dimensional carbon material, has attracted attention owing to its remarkable electronic properties [1], including high carrier mobility, low spin-orbit coupling [2], and so on. These unique characteristics make graphene a promising candidate for high-performance quantum devices [3], such as quantum dots with long relaxation time [4, 5].

Quantum dots, called artificial atoms owing to their discrete energy levels and controllable electron numbers, have been investigated from both viewpoints of fundamental physics and applications [6–8]. Although optical measurements have been the primary tool to investigate physically defined nanoscale quantum dots such as colloidal systems [9–11], advances in nanotechnology have enabled the fabrication of electrical contacts to individual quantum dots, allowing for direct transport measurements. This electrical approach to colloidal quantum dot systems has demonstrated their potential as single-electron transistors operating at room temperatures, opening new frontiers in quantum device applications [12].

To create such nanoscale structures in graphene, chemical vapor deposition (CVD), typically known as a large-scale synthesis method, can be utilized [13–16]. The CVD growth is utilized not only to fabricate graphene nanoribbon [17–19] but also self-assembled graphene nanoislands (GNIs) which can be unexpectedly formed with nanoscale dimensions. The electronic properties of these GNIs have been investigated by scanning tunneling microscopy (STM), revealing discrete density of states [20] and pseudo-magnetic field effect [21, 22]. However, while these STM studies suggest the potential of graphene nanoislands for quantum devices, the actual device fabrication and measurement of the devices have been challenging. This is because typical CVD methods to deposit graphene require metal substrate catalysts,

which induce parallel current paths through the substrates. Although catalyst-free CVD methods have been previously explored and electrical measurements of larger single-layer graphene domains have been achieved [23], quantum effects in these structures have not been reported.

In this study, we demonstrate direct electrical measurements of graphene nanoislands deposited by a catalyst-free CVD growth method directly on Si/SiO₂ substrates. This approach enables us to fabricate metal electrodes on substrates contacting fine structures of graphene, allowing us to measure quantum transport properties of GNI at low temperatures.

Figure 1(a) illustrates the concept of electrical measurements. We perform microwave plasma CVD to synthesize graphene layers on 300 mm Si/SiO₂ substrates below the temperature of 400°C [24]. The Ti/Au source and drain electrodes are deposited on GNIs directly grown on Si/SiO₂ substrates by and electron beam deposition and lithography. The width of gaps between source and drain electrodes is designed to range from 20 to 80 nm. We also align a side gate electrode near the gap. GNIs are randomly created on the substrates and contacted in the electrode gaps, as shown in the scanning electron microscope (SEM) image of a typical device in Fig. 1(b). In successful cases, we can obtain a source-drain current I_{sd} at room temperature as shown in Fig. 1(c). Figure 1(d) summarizes the number of devices achieving electrical contact to GNIs. The device states are classified based on room temperature measurements without gate voltage. Devices with resistance above 100 M Ω are considered electrically open, those with resistance below tens of k Ω are classified as electrical shorts, and contacts typically show resistance ranging from 0.1 to several M Ω . The contact yield is approximately 0.1 for all gap sizes. In particular, gaps designed as 20 nm show

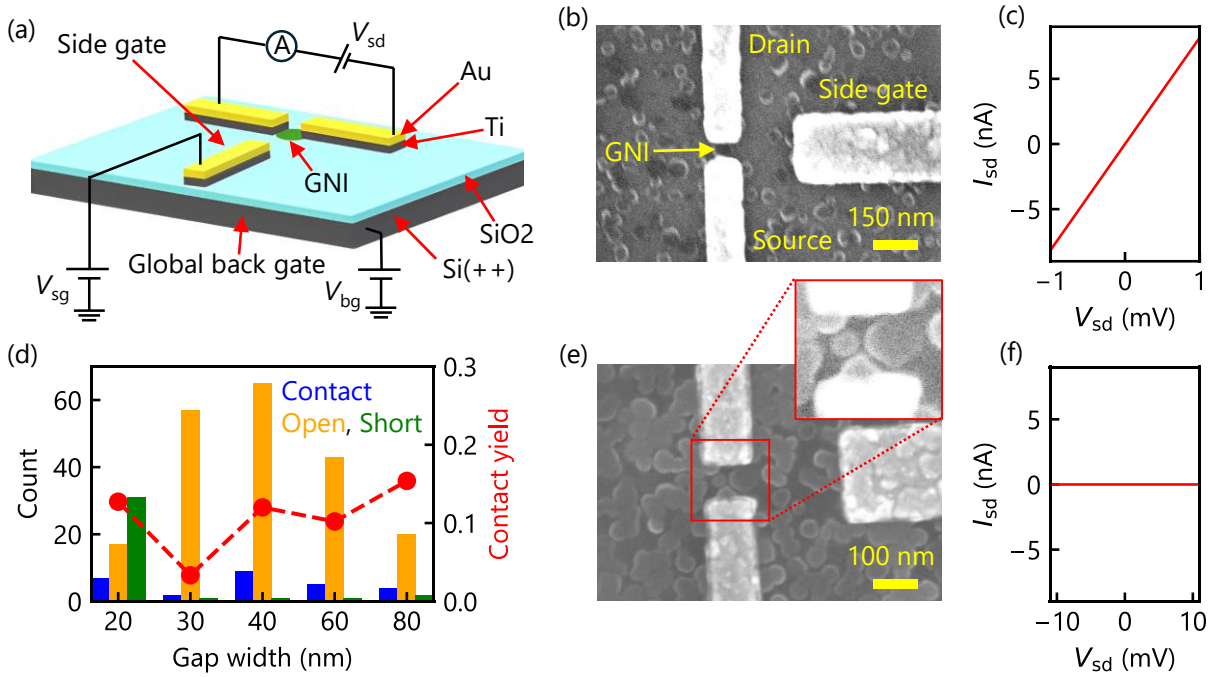


FIG. 1. (a) Schematic of the device structure. (b) Scanning electron microscope (SEM) image of a fabricated device where both electrodes are in contact with the GNI. (c) Typical I_{sd} - V_{sd} characteristics for devices classified as contacts. (d) Number of devices showing electrical contact, open, and short to GNIs. (e) SEM image of a device showing an electrical open circuit. (f) Typical I_{sd} - V_{sd} characteristics for an electrical open.

31 cases of electrical shorts due to their narrow width. Most devices result in electrical open circuits, with typical SEM images and transport characteristics shown in Figs. 1(e) and (f). As clearly seen, GNIs are not connected to each other, resulting in electrical open. These results highlight a fundamental challenge in the electrical measurement of GNIs. We need smaller GNIs to observe quantum effects, achieving electrical contact to such small GNIs requires narrower electrode gaps, which increases the probability of electrical shorts as demonstrated in this study. For our devices, we fabricate the electrodes using electron beam lithography. Here, alternative approaches such as electrical break junction techniques could potentially provide more precise control over nanogap formation [25–27], offering a promising direction for future device fabrication.

To explore quantum effects, we measure the transport characteristics at a low temperature of 2 K using a helium decompression refrigerator. Figures 2(a) and (b) show I_{sd} - V_{sd} curves at back gate voltages V_{bg} of -3.75 and -2.25 V, respectively. While we observe an Ohmic-like behavior at $V_{bg} = -3.75$ V, a suppressed current region appears at $V_{bg} = -2.25$ V. Figure 2(c) shows dI_{sd}/dV_{sd} normalized by the conductance quantum e^2/h as a function of V_{sd} and V_{bg} . A clear diamond shape appears in the figure, known as a Coulomb diamond, indicating quantum dot formation.

We also measure the Coulomb diamond by sweeping the side gate voltage V_{sg} , as shown in Fig. 2(d), and observe

similar results to those obtained by sweeping V_{bg} . Side gate modulation provides flexibility in device design, allowing for back-gate-free structures using undoped Si substrates [28, 29]. Such structures allow us to perform radio-frequency measurements, which are important techniques for investigating quantum dynamics [30–32]. Our results suggest that GNI quantum dots can achieve quantum state control and readout by utilizing high-speed electronic techniques.

In the case of this device, the size of the Coulomb diamonds changes periodically in both measurements when sweeping V_{bg} and V_{sg} . We analyze the smallest Coulomb diamond shown in Fig. 2(c) using the constant-interaction model [8], as illustrated in Fig. 3(a). Here, C_g is the capacitance between the GNI quantum dot and gate electrode, C_s the capacitance to the source electrode, and C_d the capacitance to the drain electrode, and C the total capacitance of the device. Full depletion of carriers in GNIs cannot be observed even when applying higher gate voltages, which makes it difficult to count the exact number of carriers. Therefore, we denote N as the number of carriers, assuming electron transport. The charging energy E_c is obtained from the width of the diamond along the V_{sd} axis, giving $E_c = e^2/C$, where e is the elementary charge. The lever arm α is calculated from the ratio of C_g and C , which converts the gate voltage to the energy scales. The extracted values are summarized in Table. I. The values of C_{sg} show similar capacitance to C_{bg} and can be controlled by the side gate electrode design. The similar values of C_s

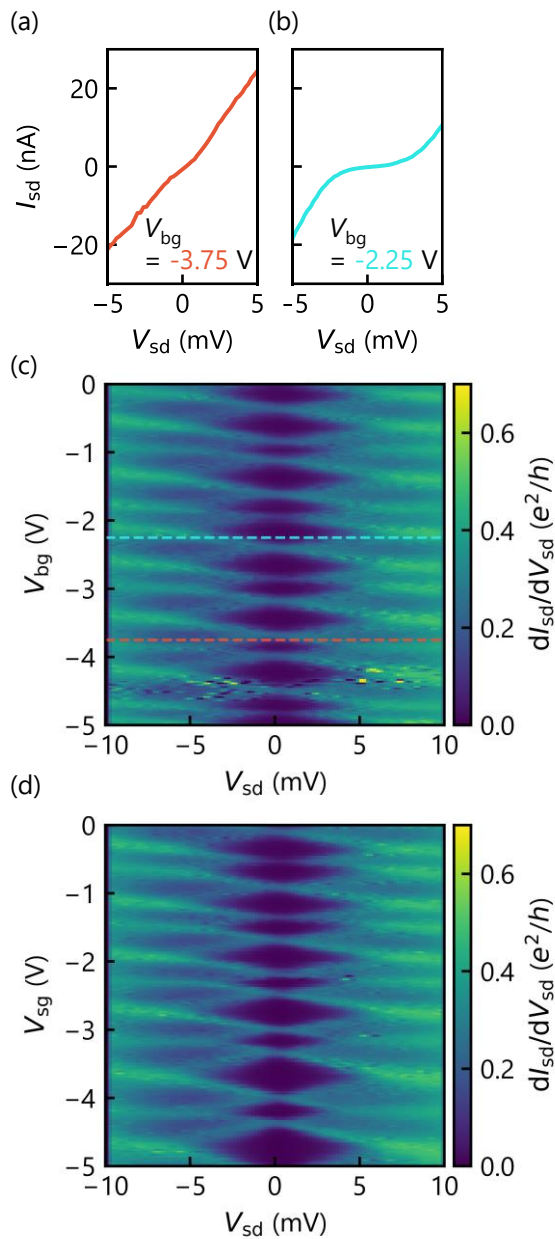


FIG. 2. (a) I_{sd} - V_{sd} characteristics at $V_{bg} = -3.75$ V and (b) at $V_{bg} = -2.25$ V measured at 2 K. (c) Differential conductance dI_{sd}/dV_{sd} as a function of V_{sd} and V_{bg} , and (d) with V_{sd} and V_{sg} .

and C_d indicate that both electrodes are deposited symmetrically on the GNI, which is reflected in the symmetric shape of the Coulomb diamonds. From C_{bg} , we estimate the quantum dot size D to be 73 nm by assuming a parallel circular plate model following $C_{bg} = \epsilon_0 \epsilon_r \pi D^2 / 4d$, where ϵ_0 is the permittivity of vacuum, $\epsilon_r = 3.9$ and $d = 285$ nm are the dielectric constant and the thickness of SiO_2 , respectively. This value is consistent with the typical size of GNIs observed in our substrates.

TABLE I. Summary of electrostatic capacitances and charging energy. The units of each capacitance and energy are given as aF and meV, respectively.

	C_g	C_s	C_d	C	$\alpha = C_g/C$	E_c
Back gate	0.5	17	14	35	0.014	4.6
Side gate	0.4	18	19	38	0.011	4.3

The difference between the shape of consecutive diamonds provides the orbital energy spacing $\Delta\epsilon(N)$, which can be extracted when the diamond size alternates between larger and smaller values. In graphene quantum dots, both valley and spin degrees of freedom typically result in a fourfold periodic pattern in the Coulomb diamond size [33]. The larger diamonds appear when electrons begin to occupy the next orbital level, requiring additional orbital energy on top of the charging energy. Figure 3(b) shows the addition energy E_{add} normalized by E_c for each electron number, where E_{add} is evaluated from the width of each diamond. We observe that E_{add} alternates with the addition of every two electrons, indicating twofold degeneracy. This suggests that the valley degeneracy has vanished in our GNI quantum dots, likely due to the low crystallinity of the GNIs. The size of the quantum dot is also estimated by considering a harmonic oscillator potential in the GNI. In this potential, the wave function is assumed to be Gaussian, and its spatial dispersion $2\hbar/\sqrt{m^* \Delta\epsilon(N)}$ corresponds to the dot size, where $m^* = 0.022m_0$ is the effective mass of bilayer graphene [34]. From this model, we evaluate the typical dot size to be 71 nm, which is in good agreement with the value obtained from the parallel circular plate model.

Figure 4(a) shows the Coulomb diamonds of another device obtained by sweeping V_{bg} . We employ Cr/Au electrodes for this device to investigate the contact metal dependence of transport characteristics. Clear diamonds are observed similar to the previously presented results, providing an estimated dot size of approximately 33 nm assuming the parallel circular plate model. All diamonds show almost identical shapes despite the dot size being small enough to expect cyclic changes in diamond size reflecting orbital energy spacing. The origin of this behavior remains unclear and requires further investigation. The shape of the diamonds is slightly rounded compared to the device shown in Fig. 2, indicating an increased tunneling rate between the quantum dot and lead electrodes. This change might be caused by the difference in work function between Cr and Ti, which modulates the barrier between the dot and electrodes. However, the device conductance is smaller than that of the previous device. The possible reason may be the asymmetry in tunnel coupling.

In conclusion, we have demonstrated electrical transport measurements of GNIs directly grown on SiO_2 substrates by microwave plasma CVD method. Owing to the catalyst-free CVD growth, we fabricate metal electrodes directly on the GNIs. Low-temperature measurements reveal clear Coulomb diamonds, indicating the formation of quantum dots. The Coulomb diamonds of the presented device show twofold

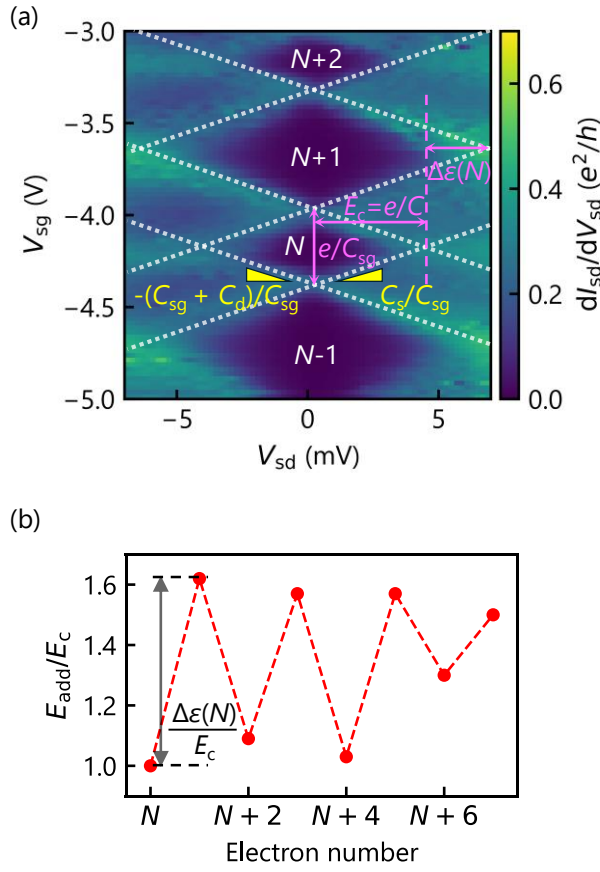


FIG. 3. (a) Enlarged view of Coulomb diamonds obtained by sweeping V_{sg} , and analysis guideline for the constant-interaction model. (b) The addition energy normalized by the charging energy as a function of electron number from N to $N + 7$.

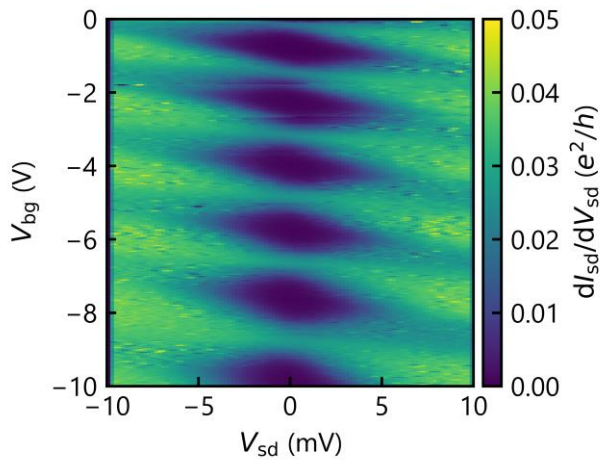


FIG. 4. Coulomb diamonds obtained from another device with Cr/Au contacts by sweeping V_{bg} .

degeneracy instead of the fourfold degeneracy typically observed in graphene quantum dots, suggesting the vanishing of valley degeneracy due to the low crystallinity of GNIs. The dependence on contact metals shows that the tunneling coupling between leads and quantum dots can be controlled through material selection. Our results show that GNI quantum dots can utilize radio-frequency techniques and possess tunability of tunnel coupling by optimizing device structure design. Furthermore, all processes to fabricate devices, including graphene synthesis, are performed below 400°C , making our approach suitable for semiconductor integration. These findings provide not only fundamental insights into the quantum transport properties of GNIs but also device design guidelines to realize quantum computing.

ACKNOWLEDGEMENTS

We thank RIEC Fundamental Technology Center and the Laboratory for Nanoelectronics and Spintronics for technical support. Part of this work is supported by Grants-in-Aid for Scientific Research (21K18592, 23K26482, 23H04490, 25H01504, 25H02106), CREST (JPMJCR23A2), JST, and FRiD Tohoku University.

COMPETING INTERESTS

The authors declare no competing interests.

* These authors contributed equally to this work

† tomohiro.otsuka@tohoku.ac.jp

- [1] K. S. Novoselov, A. K. Geim, S. V. Morozov, D.-e. Jiang, Y. Zhang, S. V. Dubonos, I. V. Grigorieva, and A. A. Firsov, Electric field effect in atomically thin carbon films, *Science* **306**, 666 (2004).
- [2] D. Huertas-Hernando, F. Guinea, and A. Brataas, Spin-orbit coupling in curved graphene, fullerenes, nanotubes, and nanotube caps, *Phys. Rev. B* **74**, 155426 (2006).
- [3] B. Trauzettel, D. V. Bulaev, D. Loss, and G. Burkard, Spin qubits in graphene quantum dots, *Nature Physics* **3**, 192 (2007).
- [4] L. Banszerus, K. Hecker, S. Möller, E. Icking, K. Watanabe, T. Taniguchi, C. Volk, and C. Stampfer, Spin relaxation in a single-electron graphene quantum dot, *Nat. Commun.* **13**, 3637 (2022).
- [5] R. Garreis, C. Tong, J. Terle, M. J. Ruckriegel, J. D. Gerber, L. M. Gächter, K. Watanabe, T. Taniguchi, T. Ihn, K. Ensslin, and W. W. Huang, Long-lived valley states in bilayer graphene quantum dots, *Nat. Phys.* **20**, 428 (2024).
- [6] S. Tarucha, D. Austing, T. Honda, R. Van der Hage, and L. P. Kouwenhoven, Shell filling and spin effects in a few electron quantum dot, *Phys. Rev. Lett.* **77**, 3613 (1996).
- [7] L. P. Kouwenhoven, T. Oosterkamp, M. Danoesastro, M. Eto, D. Austing, T. Honda, and S. Tarucha, Excitation spectra of circular, few-electron quantum dots, *Science* **278**, 1788 (1997).
- [8] L. P. Kouwenhoven, D. Austing, and S. Tarucha, Few-electron quantum dots, *Rep. Prog. Phys.* **64**, 701 (2001).

- [9] D. Press, T. D. Ladd, B. Zhang, and Y. Yamamoto, Complete quantum control of a single quantum dot spin using ultrafast optical pulses, *Nature* **456**, 218 (2008).
- [10] R. J. Warburton, Single spins in self-assembled quantum dots, *Nat. Mater.* **12**, 483 (2013).
- [11] D. Tian, H. Ma, G. Huang, M. Gao, F. Cai, Y. Fang, C. Li, X. Jiang, A. Wang, S. Wang, and Z. Du, A Review on Quantum Dot Light-Emitting Diodes: From Materials to Applications, *Adv. Optical Mater.* **11**, 2201965 (2023).
- [12] K. Shibata, M. Yoshida, K. Hirakawa, T. Otsuka, S. Z. Bisri, and Y. Iwasa, Single PbS colloidal quantum dot transistors, *Nat. Commun.* **14**, 7486 (2023).
- [13] Q. Yu, J. Lian, S. Siriponglert, H. Li, Y. P. Chen, and S.-S. Pei, Graphene segregated on Ni surfaces and transferred to insulators, *Appl. Phys. Lett.* **93** (2008).
- [14] A. Reina, X. Jia, J. Ho, D. Nezich, H. Son, V. Bulovic, M. S. Dresselhaus, and J. Kong, Large area, few-layer graphene films on arbitrary substrates by chemical vapor deposition, *Nano Lett.* **9**, 30 (2009).
- [15] X. Li, W. Cai, J. An, S. Kim, J. Nah, D. Yang, R. Piner, A. Vellamakanni, I. Jung, E. Tutuc, S. K. Banerjee, L. Colombo, and R. S. Ruoff, Large-area synthesis of high-quality and uniform graphene films on copper foils, *Science* **324**, 1312 (2009).
- [16] H. Ago, Y. Ogawa, M. Tsuji, S. Mizuno, and H. Hibino, Catalytic growth of graphene: toward large-area single-crystalline graphene, *J. Phys. Chem. Lett.* **3**, 2228 (2012).
- [17] T. Kato and R. Hatakeyama, Site-and alignment-controlled growth of graphene nanoribbons from nickel nanobars, *Nat. Nanotechnol.* **7**, 651 (2012).
- [18] H. Suzuki, T. Kaneko, Y. Shibuta, M. Ohno, Y. Maekawa, and T. Kato, Wafer-scale fabrication and growth dynamics of suspended graphene nanoribbon arrays, *Nature Commun.* **7**, 11797 (2016).
- [19] T. Kato, T. Kitada, M. Seo, W. Okita, N. Sato, M. Shinozaki, T. Abe, T. Kumasaka, T. Aizawa, Y. Muto, T. Kaneko, and T. Otsuka, Scalable fabrication of graphene nanoribbon quantum dot devices with stable orbital-level spacing, *Commun. Mater.* **3**, 103 (2022).
- [20] S.-h. Phark, J. Borme, A. L. Vanegas, M. Corbetta, D. Sander, and J. Kirschner, Scanning tunneling spectroscopy of epitaxial graphene nanoisland on Ir (111), *Nanoscale Res. Lett.* **7**, 1 (2012).
- [21] N. Levy, S. Burke, K. Meaker, M. Panlasigui, A. Zettl, F. Guinea, A. C. Neto, and M. F. Crommie, Strain-induced pseudo-magnetic fields greater than 300 tesla in graphene nanobubbles, *Science* **329**, 544 (2010).
- [22] M. Settnes, S. R. Power, and A.-P. Jauho, Pseudomagnetic fields and triaxial strain in graphene, *Phys. Rev. B* **93**, 035456 (2016).
- [23] D. Wei, Y. Lu, C. Han, T. Niu, W. Chen, and A. T. S. Wee, Critical crystal growth of graphene on dielectric substrates at low temperature for electronic devices., *Angew. Chem., Int. Ed.* **52**, 14121 (2013).
- [24] T. Yamada, J. Kim, M. Ishihara, and M. Hasegawa, Low-temperature graphene synthesis using microwave plasma cvd, *J. Phys. D: Appl. Phys.* **46**, 063001 (2013).
- [25] H. Park, A. K. Lim, A. P. Alivisatos, J. Park, and P. L. McEuen, Fabrication of metallic electrodes with nanometer separation by electromigration, *Appl. Phys. Lett.* **75**, 301 (1999).
- [26] D. Strachan, D. Smith, D. Johnston, T.-H. Park, M. J. Therien, D. Bonnell, and A. Johnson, Controlled fabrication of nanogaps in ambient environment for molecular electronics, *Appl. Phys. Lett.* **86** (2005).
- [27] V. Dubois, S. N. Raja, P. Gehring, S. Caneva, H. S. van der Zant, F. Niklaus, and G. Stemme, Massively parallel fabrication of crack-defined gold break junctions featuring sub-3 nm gaps for molecular devices, *Nat. Commun.* **9**, 3433 (2018).
- [28] T. Johmen, M. Shinozaki, Y. Fujiwara, T. Aizawa, and T. Otsuka, Radio-Frequency Reflectometry in Bilayer Graphene Devices Utilizing Microscale Graphite Back-Gates, *Phys. Rev. Appl.* **20**, 014035 (2023).
- [29] M. J. Ruckriegel, L. M. Gächter, D. Kealhofer, M. Bahrami Panah, C. Tong, C. Adam, M. Masseroni, H. Duprez, R. Garreis, K. Watanabe, T. Taniguchi, A. Wallraff, T. Ihn, K. Ensslin, and W. W. Huang, Electric dipole coupling of a bilayer graphene quantum dot to a high-impedance microwave resonator, *Nano Lett.* **24**, 7508 (2024).
- [30] H. Qin and D. A. Williams, Radio-frequency point-contact electrometer, *Appl. Phys. Lett.* **88**, 203506 (2006).
- [31] D. Reilly, C. Marcus, M. Hanson, and A. Gossard, Fast single-charge sensing with a rf quantum point contact, *Appl. Phys. Lett.* **91**, 162101 (2007).
- [32] C. Barthel, D. Reilly, C. M. Marcus, M. Hanson, and A. Gossard, Rapid single-shot measurement of a singlet-triplet qubit, *Phys. Rev. Lett.* **103**, 160503 (2009).
- [33] A. Kurzman, Y. Kleorin, C. Tong, R. Garreis, A. Knothe, M. Eich, C. Mittag, C. Gold, F. K. de Vries, K. Watanabe, T. Taniguchi, V. Fal'ko, Y. Meir, T. Ihn, and K. Ensslin, Kondo effect and spin-orbit coupling in graphene quantum dots, *Nat. Commun.* **12**, 6004 (2021).
- [34] J. Li, L. Z. Tan, K. Zou, A. A. Stabile, D. J. Seiwel, K. Watanabe, T. Taniguchi, S. G. Louie, and J. Zhu, Effective mass in bilayer graphene at low carrier densities: The role of potential disorder and electron-electron interaction, *Phys. Rev. B* **94**, 161406 (2016).